Supporting Information

Kerr gated Raman spectroscopy of $LiPF_6$ salt and $LiPF_6$-based organic carbonate electrolyte for Li-ion batteries

Laura Cabo-Fernandez,[a] Alex R. Neale,[a] Filipe Braga,[a] Igor V. Sazanovich,[b]
Robert Kostecki,[c] Laurence J. Hardwick*[a]

[a] Stephenson Institute for Renewable Energy, Department of Chemistry, University of Liverpool, Peach Street, Liverpool, L69 7ZF (United Kingdom).

[b] Central Laser Facility, Research Complex at Harwell, STFC Rutherford Appleton Laboratory, Harwell Campus, Didcot, Oxfordshire, OX11 0QX (United Kingdom).

[c] Environmental Energy Technologies Division, Lawrence Berkeley National Laboratory, Berkeley, CA 94720 (United States).

* hardwick@liverpool.ac.uk

Principles of Raman spectroscopy

When a sample is lightened by a laser, the molecule interacts with the incident photon through the virtual energy level and then another photon is scattered; therefore, scattering processes can be looked at as the absorption of one photon and the instantaneous emission of another photon. The process is elastic if the scattered photon has the same energy as the incident one ($E_s=E_i$), in which case it is known as Rayleigh scattering, or if both photons have different energy ($E_s \neq E_i$) it is an inelastic process. Raman spectroscopy is based on these inelastic phenomena and it could be a Stokes scattering if the scattered photon has less energy than the incident one ($E_s < E_i$) or if it has more energy ($E_s > E_i$) an anti-Stokes scattering, as seen in **Figure 1 (a)**.

Fluorescence lifetime and quantum yields[1]

Fluorescence quantum yield (*Q*) defined as the ratio of photons emitted to the number of photons absorbed[1] could be equal to 1, whereas the yield of Raman inelastic scattering can be several orders of magnitude lower.

Fluorescence quantum yield can also be expressed in terms of the lifetime of the excited state (τ_s) and the fluorescence lifetime (τ_r) as follows:[1]

$$Q = \frac{\tau_S}{\tau_r} \tag{S1}$$

And τ_r is related to the rate constant of radiative process (k_r^s), the proportional factor that relates the fluorescence intensity and the concentration of photons in the excited state S_1, which indicates that even at low concentrations of fluorescent species (e.g., 1 ppm) fluorescence can easily overwhelm Raman scattering signal making it difficult to detect and analyse.

A number of molecules of a fluorescence species (*A*) can be excited from the ground electronic state (S_0) to a higher energy electronic state (e.g., S_1, S_2…) when a photon is absorbed during a short pulse of light (at time 0). These molecules can relax back to the ground state (S_0) through radiative (i.e., fluorescence emission at a rate k_r^S) or non-radiative processes (at a rate constant k_{nr}^S) as shown in **Scheme S1**. These non-radiative processes that the molecule can undergo to relax back to the ground state are internal conversion (rate constant k_{ic}^S) and intersystem crossing (rate constant k_{isc}). Therefore, the rate of deactivation of a molecule from the excited state is:

$$k = k_r^S + k_{nr}^S \tag{S2}$$

where k_{nr}^S is the combination of the rate constant of internal conversion and intersystem crossing.

$$k_{nr}^S = k_{ic}^S + k_{isc} \tag{S3}$$

Considering these processes, the fluorescence quantum yield (Q) can be expressed in terms of the rate constants as follows:

$$Q = \frac{k_r^S}{k_r^S + k_{nr}^S} = k_r^S \tau_S \tag{S4}$$

where τ_s is the lifetime of the excited state, $\tau_S = 1/(k_r^S + k_{nr}^S)$. Q can also be written in terms of τ_s and the radiative lifetime as:

$$Q = \frac{\tau_S}{\tau_r} \tag{S5}$$

The fluorescence intensity (i_F) at a particular time (t) after excitation (t_0) is related to the concentration of excited molecules [$^1A^*$]

$$A^* \xrightarrow{k_r^S} A + photon \tag{S6}$$

$$i_F(t) = k_r^S[^1A^*] \tag{S7}$$

this equation expressed in terms of the concentration or number of photons absorbed $[^1A^*]_0$ is

$$i_F(t) = k_r^S[^1A^*]_0 exp\left(-\frac{t}{\tau_S}\right) \tag{S8}$$

This equation shows that there is proportional relation between fluorescence intensity and the concentration of excited photons. If the only process of deactivation or relaxation for the excited state (S_1) to the ground state (S_0), is through fluorescence emission, $\tau_S = 1/k_r^S$.

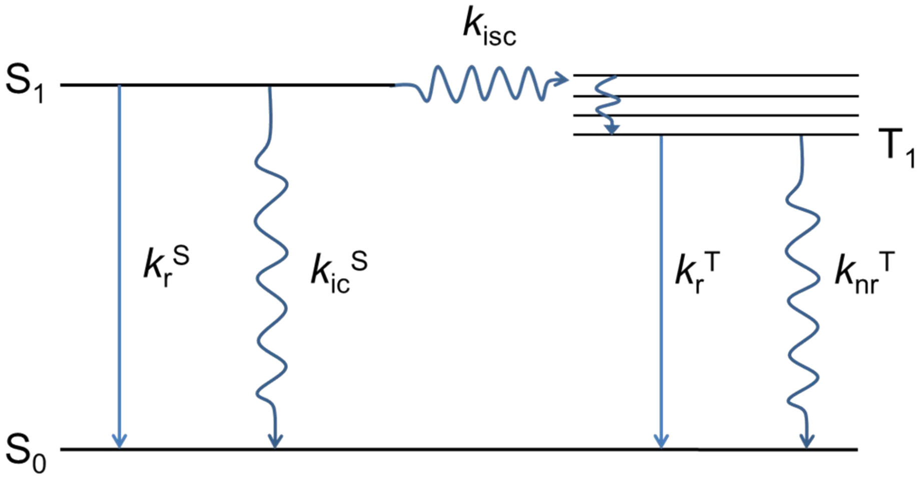

Scheme S1. Representation of the different relaxation processes of a fluorescence molecule from the excited state S_1 to the ground state S_0.[1]

In this analysis it has not been taking into account the possibility that the excitation to a triplet state, *T*, of the molecule and the processes that could take place as a consequence of this (e.g., phosphorescence). Only the processes that occur when a molecule is excited to a singlet state, *S*, have been considered for simplicity.

Raman of $LiPF_6$ salt

Raman measurements were run for the as-received $LiPF_6$ salt with different excitation wavelengths (e.g., 400, 532, 633 and 785 nm). **Figure S1** shows the emission-shape background of the Raman spectra, with broad features at approximately 600, 657 and 709 nm.

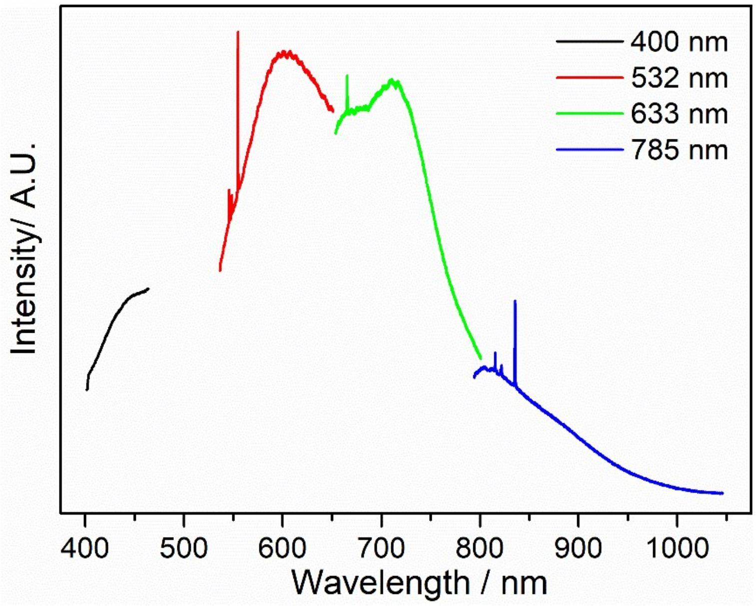

Figure S1. CW Raman spectra of $LiPF_6$ salt collected with lasers with excitation wavelengths of 400, 532, 633 and 785 nm.

Kerr gate Raman of $LiPF_6$ salt.

Kerr gate Raman spectrum of $LiPF_6$ salt was baseline corrected and the peaks have been fitted using Lorentzian function (listed in **Table S1**). The broad feature at ca. 400 cm^{-1} is attributable to the quartz cuvette (**Figure S4**).

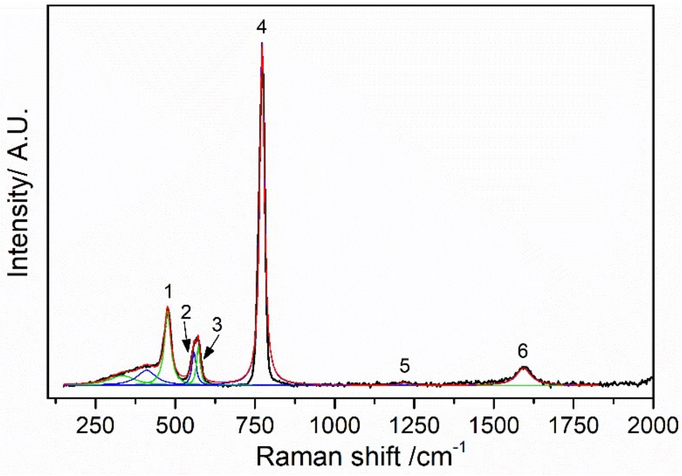

Figure S2. Lorentzian peak fitting after baseline correction of Kerr gate Raman spectrum of (a) pristine and (b) contaminated $LiPF_6$ salt collected with a laser wavelength of 400 nm.

Fourier-transform Raman of $LiPF_6$ salt

The FT-Raman spectrum of $LiPF_6$ salt was measured. Subsequently, the spectrum was baseline corrected and the peaks have been fitted using Lorentzian function (listed in **Table S1**).

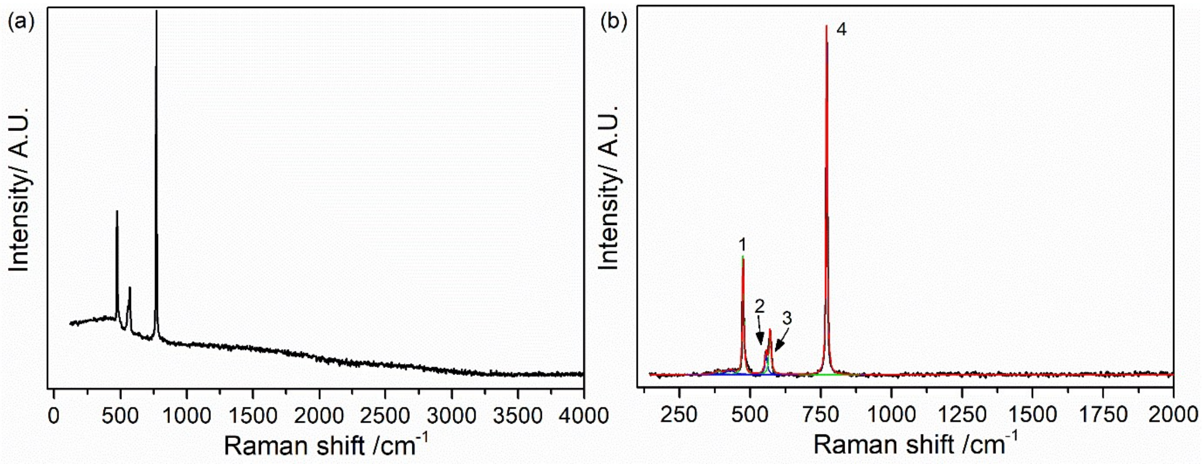

Figure S3. (a) As measured spectrum (b) Lorentzian peak fitting after baseline correction of FT-Raman spectrum of $LiPF_6$ salt collected with a laser wavelength of 1064 nm.

Table S1 Lorentzian fitting of Raman peaks observed in the spectra for $LiPF_6$ salt (**Figure S2 and S3**) obtained with 400 nm (Kerr gated) and 1064 nm lasers and their assignments.

*The T_{1U} infrared active band is also observed in the Raman due to crystal symmetry distortions.

Peak	400 nm Position/ cm^{-1}	Peak	1064 nm Position/ cm^{-1}	Assignment
1	475	1	475	E_g,
2	559	2	557	(T_{1u})*
3	572	3	570	T_{2g}
4	772	4	771	A_{1g}
5	1217			--
6	1593			--

Measurement of Quartz Cuvette

Samples were sealed inside of a quartz cuvette to carry out Raman measurements. Prior to running the samples, it was measured the cuvette under Kerr gated conditions to determine if it gives any spectroscopic signal that could interfere with the sample analysis. **Figure S4(a)** shows the Kerr-gated spectrum of the cuvette and **Figure S5** the spectrum obtained for FT-Raman with 1064 nm laser wavelength. The positions for fitted peak **(Figure S4(b)**) are collated in **Table S2**. During sample analysis, the spectrum of the cuvette was subtracted, thus there is no contribution of the sealed cell in the spectra shown for the sample and the addition peaks observed are related to products formed during $LiPF_6$ decomposition reactions.

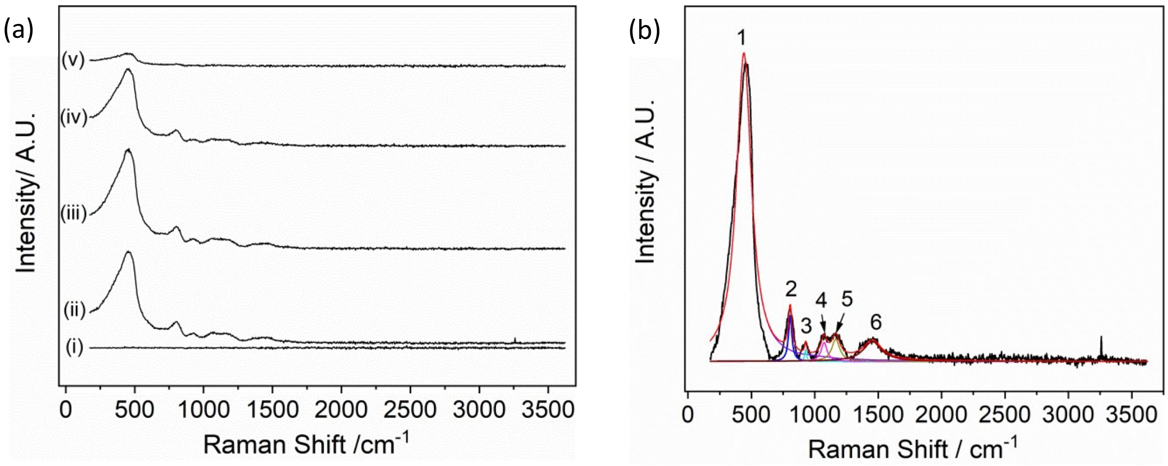

Figure S4. (a) Kerr gated Raman spectra of quartz cuvette collected at several delay times (i) -100 ps, (ii) 0 ps, (iii) 2 ps, (iv) 5 ps and (v) 10 ps; (b) Lorentzian fitting of Kerr-gated spectrum of quartz cuvette collected at 0 ps delay time.

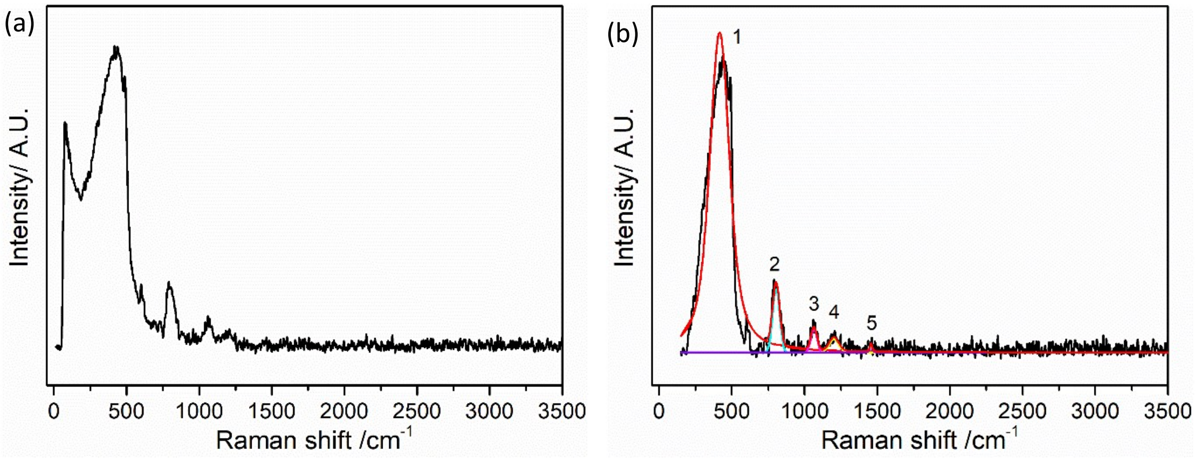

Figure S5. (a) As measured spectrum (b) Lorentzian peak fitting after baseline correction of FT-Raman spectrum of the quartz cuvette collected with a laser wavelength of 1064 nm.

Table S2. Lorentzian fitting of Raman peaks for quartz cuvette from **Figure S4 (b**) and **Figure S5 (b)**.

Kerr gated Raman (400 nm)		**FT-Raman (1064 nm)**	
Peak	**Position/ cm^{-1}**	**Peak**	**Position/cm^{-1}**
1	441	1	415
2	806	2	804
3	927	-	~ 927
4	1073	3	1064
5	1164	4	1202
6	1455	5	1456

Raman of the carbonate-based electrolyte 1 M $LiPF_6$ in EC/DMC mixture

Raman measurements were run for the conventional electrolyte 1 M $LiPF_6$ in EC/DMC mixture (1:1 w/w) with different excitation wavelengths (e.g., 400, 532, 633 and 785 nm). **Figure S6** shows the emission-shape background of the Raman spectra. It is possible to observe peaks related to the electrolyte components; however, the baseline of the spectra has a similar shape of an emission spectrum as previously observed for $LiPF_6$ salt in **Figure S1**.

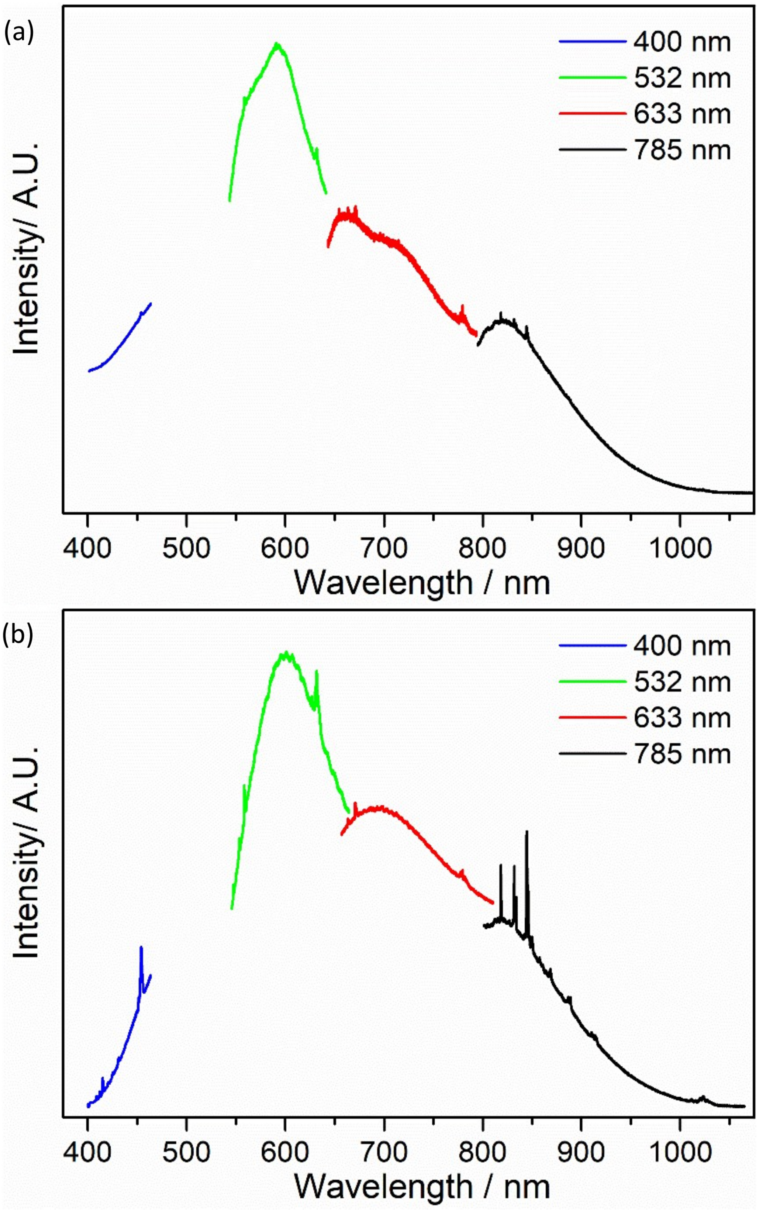

Figure S6. CW Raman spectra of (a) commercial and (b) freshly made 1M $LiPF_6$ in EC/DMC (1:1 w/w) electrolyte collected with lasers with excitation wavelengths of 400, 532, 633 and 785 nm.

Raman measurements of electrolyte components

CW Raman spectra for the electrolyte solvents DMC and EC were collected using three lasers with 400, 532, 633,785 and 1064 nm wavelengths as shown in **Figure S7**. The spectra allow us to assign the peaks in the electrolyte to each of the solvents. Since the measurements were run with five different lasers within the visible and infrared spectrum, it is possible to observe the influence of the excitation wavelength on the background emission and peak intensities. The peak positions are summarised in **Table S3**.

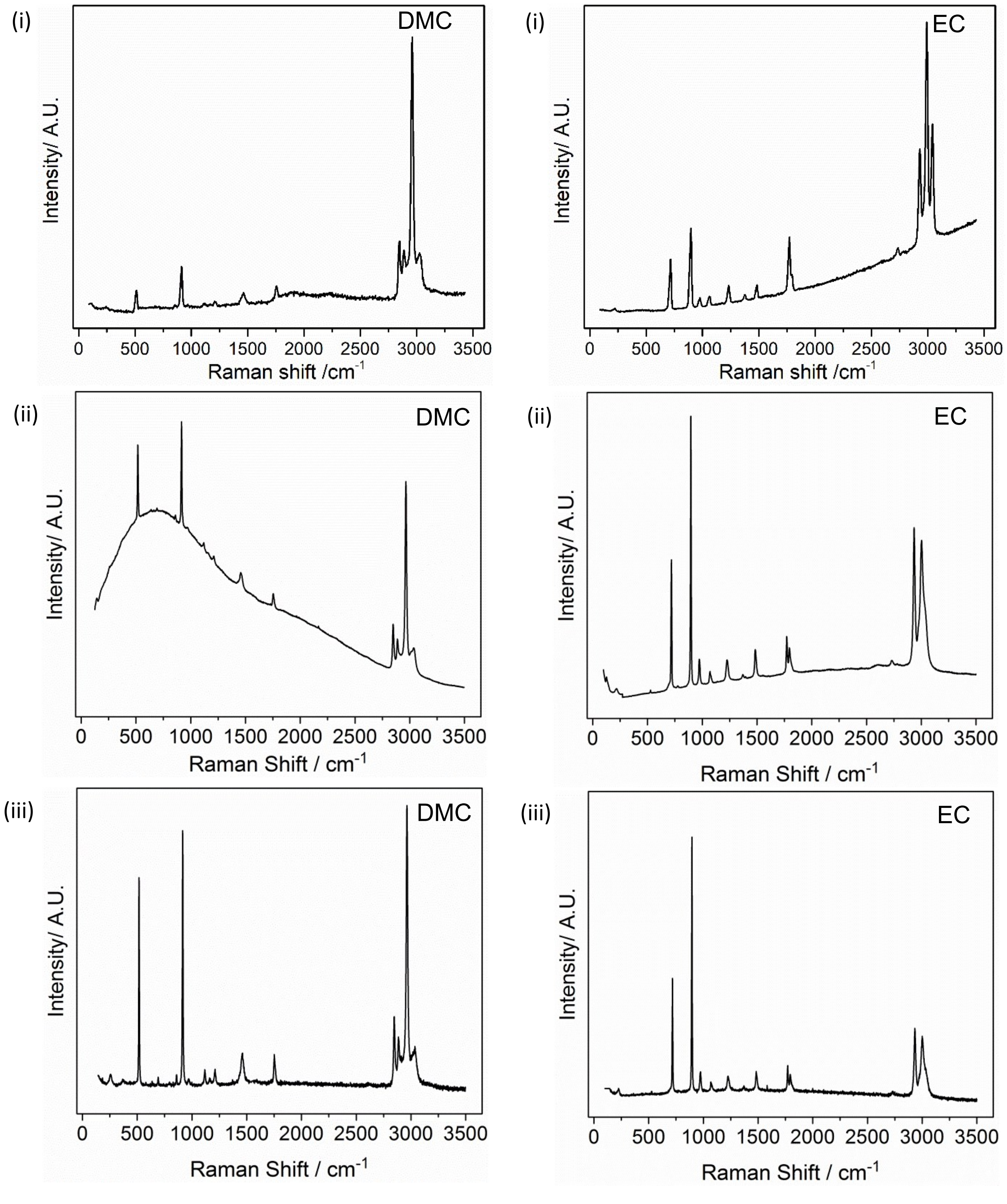

Figure S7. CW Raman spectra of DMC and EC collected with laser (i) 400 (i) 532 nm, (iii) 633 nm and (iv) 785 nm and (v) 1064 nm.

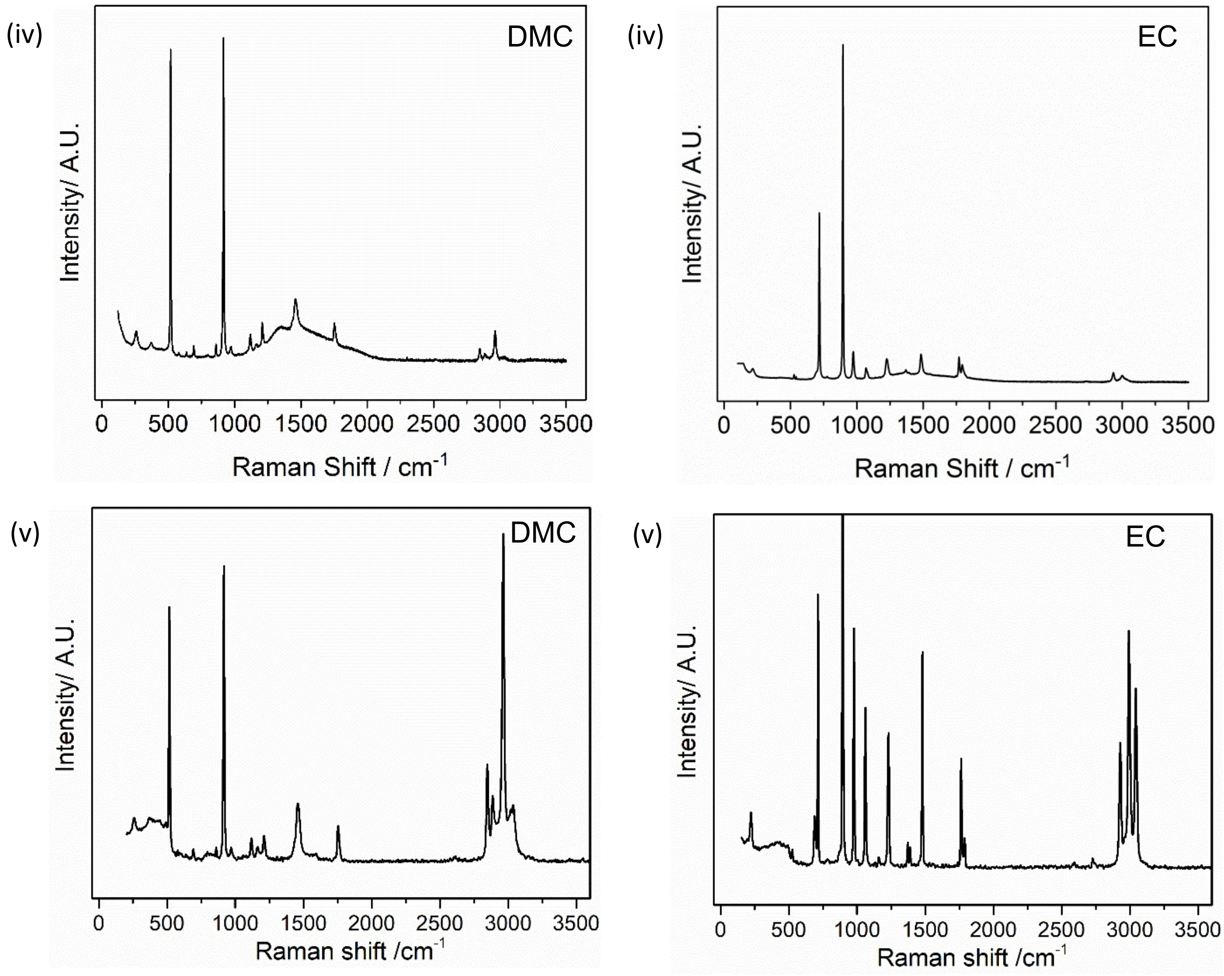

Figure S7 (continuation). CW Raman spectra of DMC and EC collected with laser (i) 400 (i) 532 nm, (iii) 633 nm and (iv) 785 nm and (v) 1064 nm.

It can be observed the there is a degree of background emission in the DMC spectrum collected with laser 532 nm. However, it is not visible in the 633 and 785 nm spectra. It can also be seen that the peak intensity of the bands associated to C-H stretching are weaker in the 785 nm spectrum in comparison with the scattering bands at lower wavenumbers with the laser wavelengths. This highlights that $LiPF_6$ (minor degradation component) is the origin of the fluorescence observed with in the battery electrolyte.

Table S3. Position of the Raman peaks (cm^{-1}) of DMC and EC solvents in the spectrum collected with 400, 532, 633, 785 and 1064 nm laser wavelengths.

Laser	400 nm	532 nm	633 nm	785 nm	1064 nm
DMC	-	258	257	259	259
	-	367	373	371	371
	513	517	517	518	517
	-	--	--	581	578
	-	636	635	639	-
	-	691	692	692	692
	856	861	860	860	860
	912	916	915	917	916
	969	972	972	974	968
	1119	1119	1119	1119	1119
	-	1162	1165	1165	1163
	1207	1211	1211	1208	1211
	1464	1458	1463	1458	1458
	1758	1752	1752	1752	1753
	2848	2848	2846	2849	2848
	2887	2889	2886	2888	2887
	2961	2965	2963	2965	2964
		3010 (sh)	--	--	
	3026	3037	3036	3035	3035
EC	221	218	225	216	221
	-	528	528	528	527
	-	-	-	-	688
	719	719	718	717	713
	-	775	777	778	783
	897	897	896	896	894
	976	974	974	974	977
	1062	1071	1068	1070	1060
	1232	1227	1227	1226	1230
	1374	1370	1370	1370	1371
	-	1396	--	1393	1388
	1482	1483	1483	1484	1479
	1772	1772	1771	1771	1762
	1793	1796	1793	1795	1787
	2737	2731	2731	2731	2727
	2930	2934	2933	2934	2929
	2990	3004	3002	3001	2991
	3042	3038 (sh)	3044 (sh)	3038 (sh)	3043

Figure S8 presents the CW Raman spectra of the solvents in a 1:1 w/w ratio mixture of EC:DMC, similar as in the electrolyte, but in the absence of $LiPF_6$ salt.

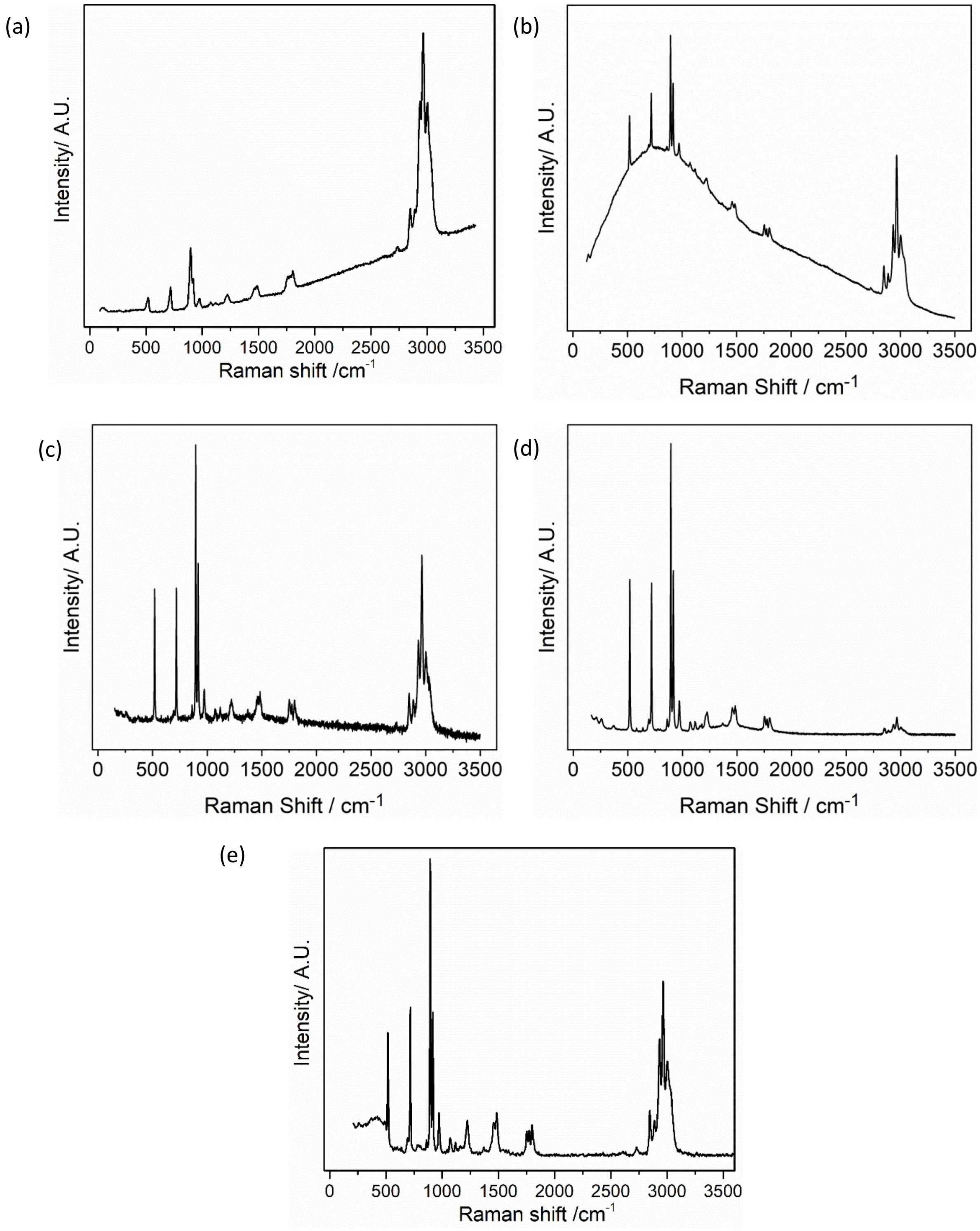

Figure S8. CW Raman spectra of DMC and EC mixture in the absence of $LiPF_6$ salt collected with laser (a) 400 nm, (b) 532 nm, (c) 633 nm and (d) 785 nm, (e) 1064 nm.

Figure S9 shows the combination of the individual spectrum of each of the solvents and in the 1:1 w/w mixture collected with each of the laser wavelengths in the same graph. This allows to determine what components of the electrolyte are mostly affected by the water contamination in the electrolyte.

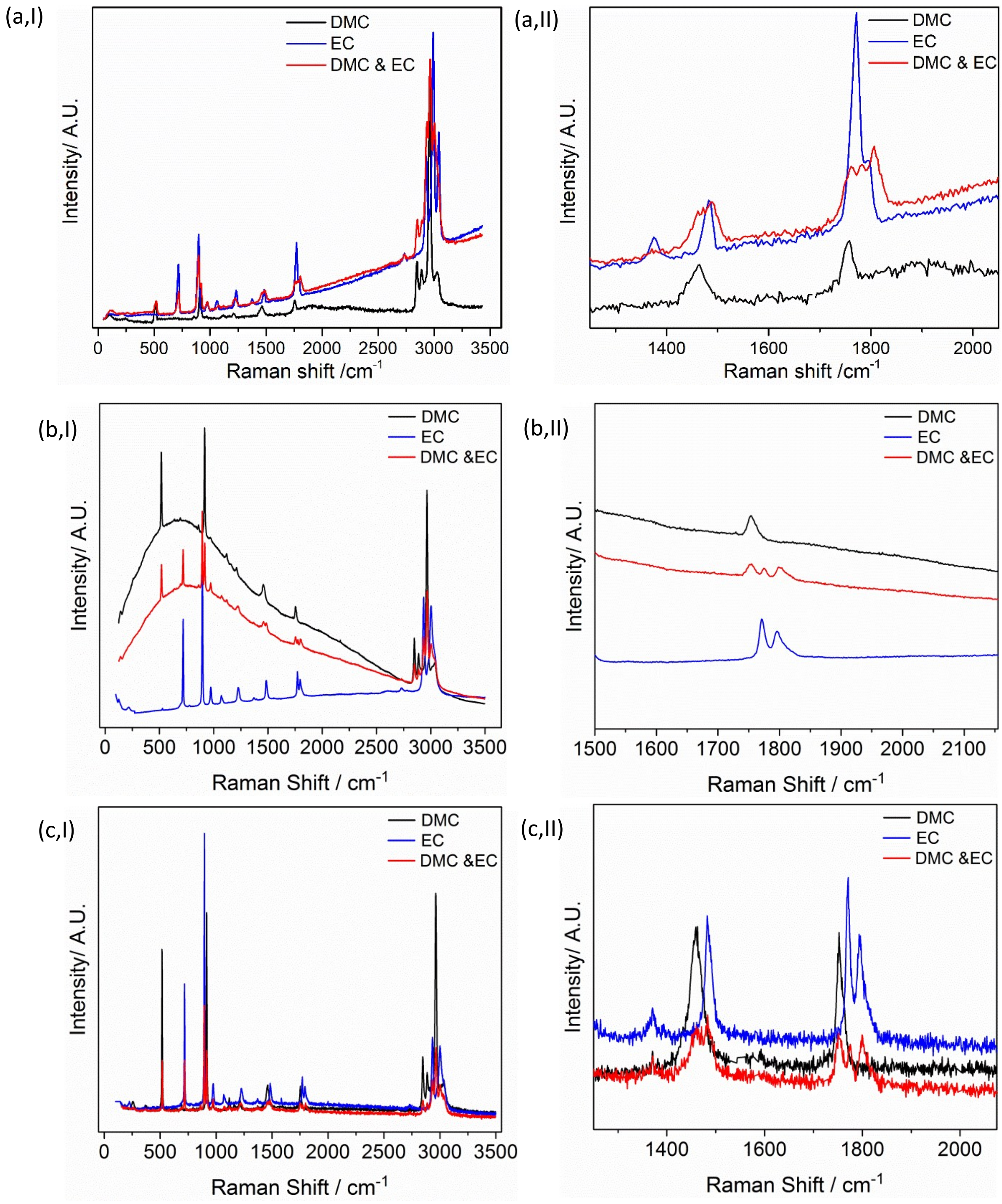

Figure S9. Comparison of (CW) Raman spectra of DMC, EC and their mixture in the absence of $LiPF_6$ salt collected with laser (a) 400 nm, (b) 532 nm, (c) 633 nm, (d) 785 nm and (e) 1064 nm. Full spectrum range (I) and within the region between 1250 and 2150 cm^{-1} (II).

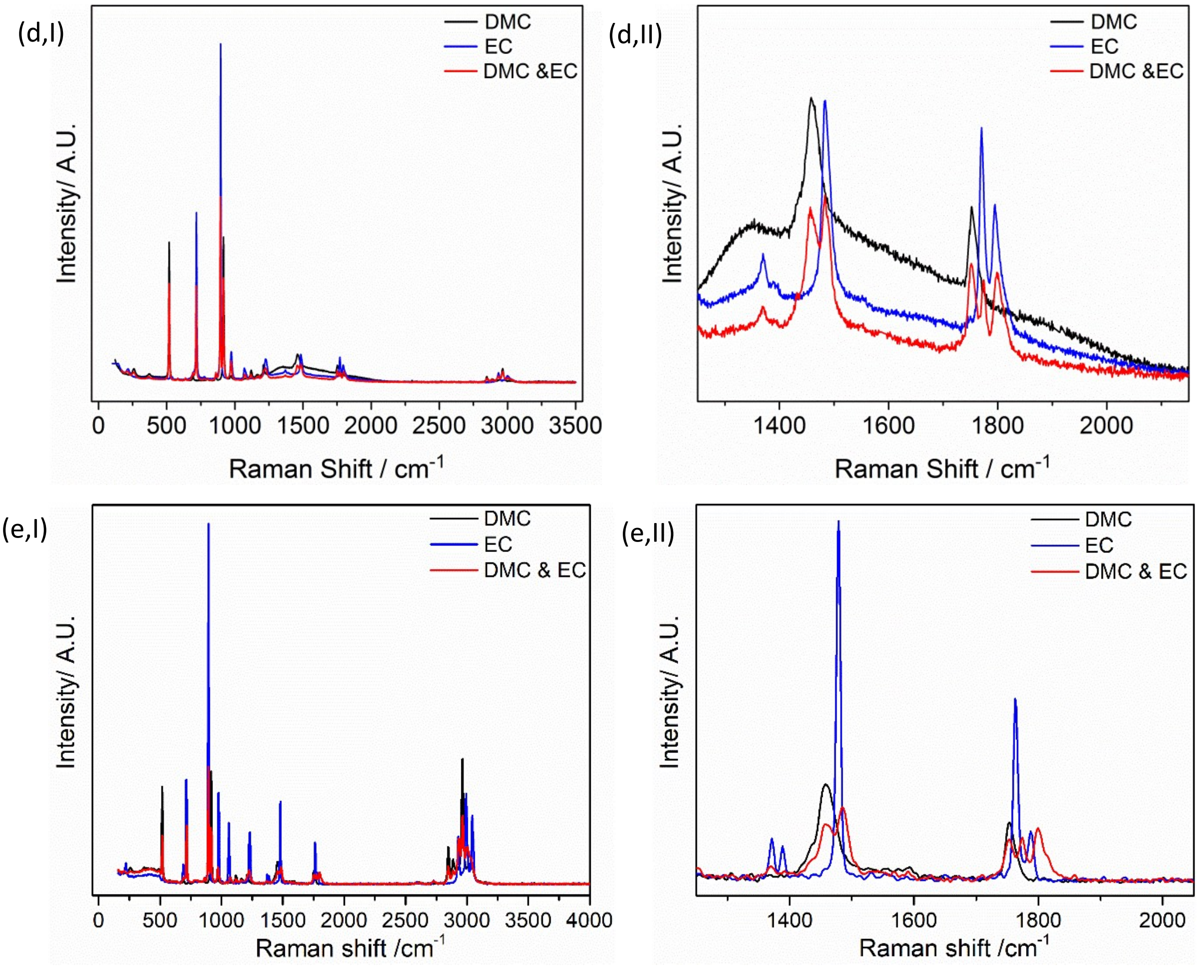

Figure S9 (continuation). Comparison of (CW) Raman spectra of DMC, EC and their mixture in the absence of $LiPF_6$ salt collected with laser (a) 400 nm, (b) 532 nm, (c) 633 nm, (d) 785 nm and (e) 1064 nm. Full spectrum range (I) and within the region between 1250 and 2150 cm^{-1} (II).

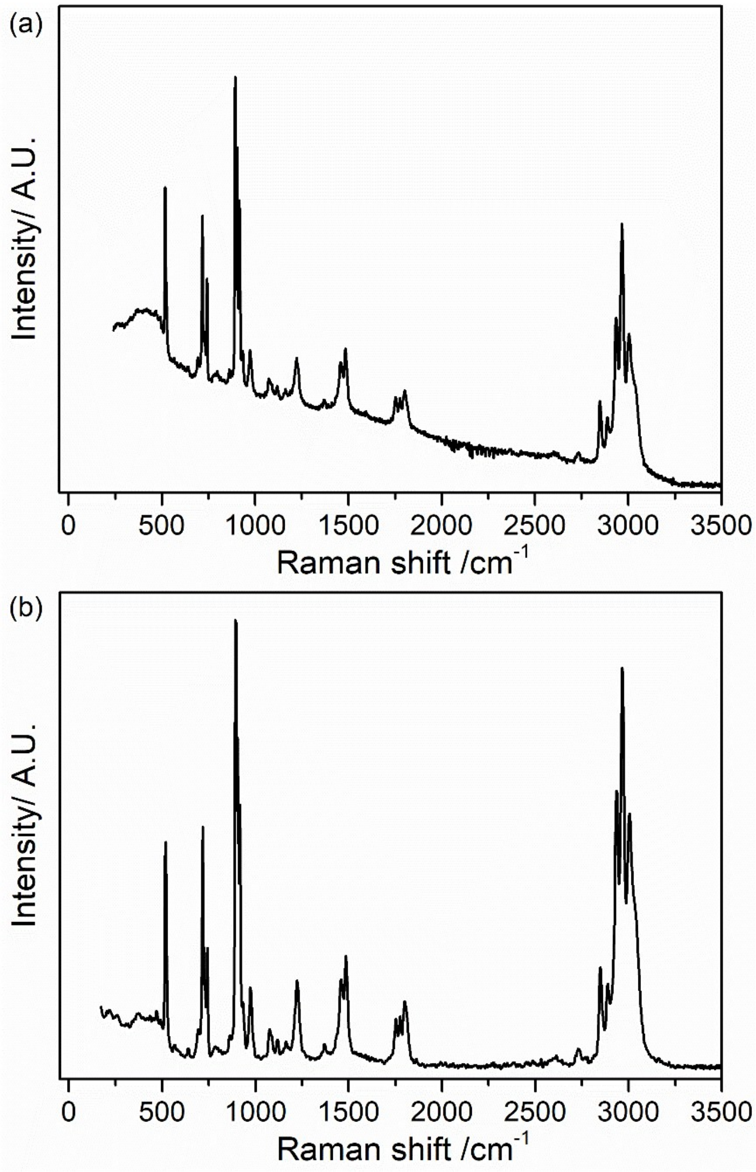

Figure S10. FT Raman spectra of (a) commercial and (b) freshly made 1M $LiPF_6$ in EC/DMC (1:1 w/w) electrolyte collected with lasers with an excitation wavelength of 1064 nm.

Kerr gated Raman measurements of aged electrolyte

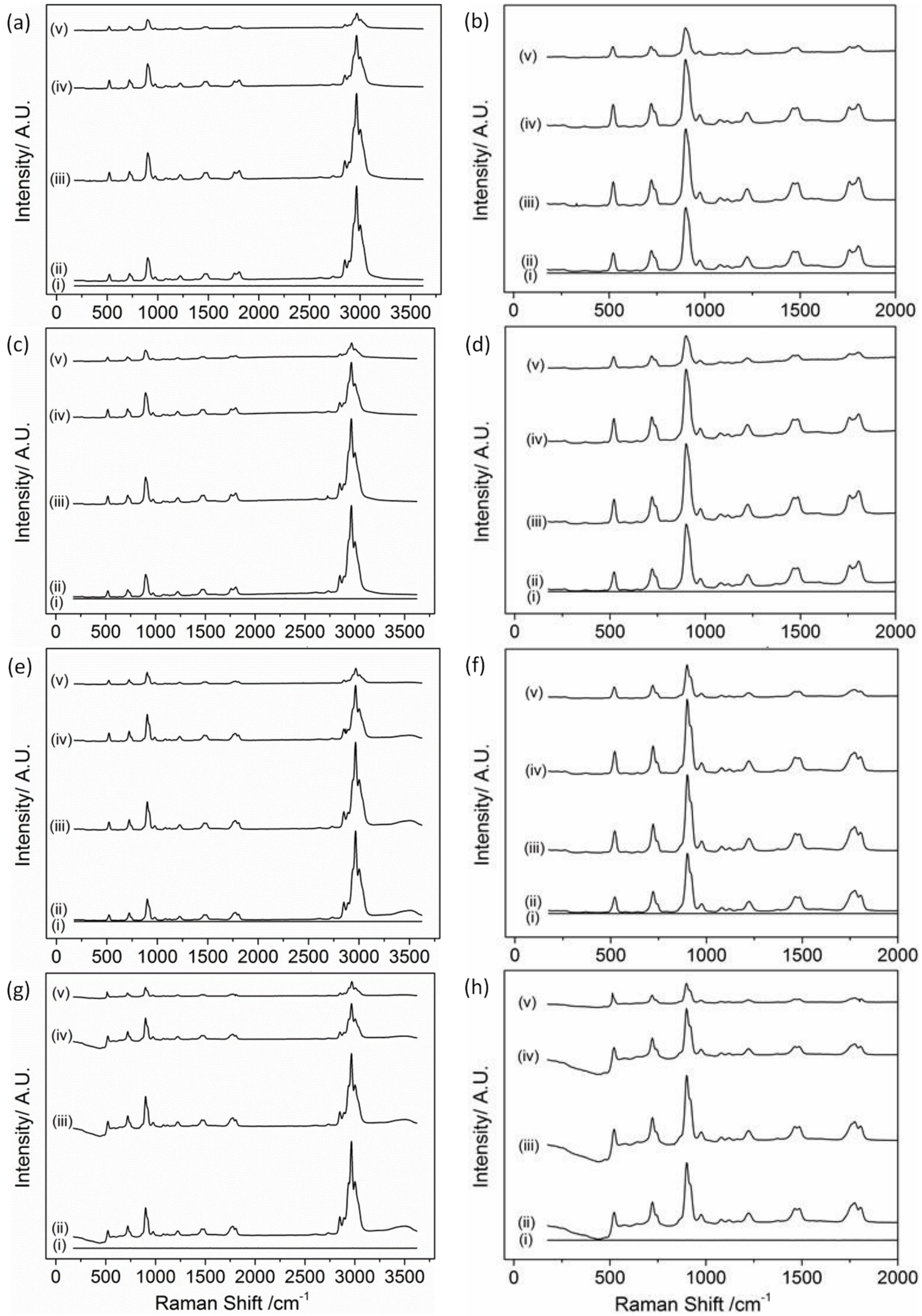

Figure S11. Kerr gate Raman spectra of commercial 1 M $LiPF_6$ in EC/DMC (1:1 w/w) electrolyte (a-b) fresh, (c-d) after 11 minutes exposure to atmosphere, (e-f) after addition of water and (g-h) after aging for 2 days in the presence of water and contact with atmosphere. Spectra were collected at several delay times (i) -100 ps, (ii) 0 ps, (iii) 2 ps, (iv) 5 ps and (v) 10 ps.

Table S4. Position and assignment of the peaks observed in Kerr gate Raman spectra and FT-Raman (1064 nm) of commercial 1 M $LiPF_6$ in EC/DMC (1:1 w/w) electrolyte.

Kerr gate Raman		**FT-Raman**	
Peak position/ cm^{-1}	**Assignment**	**Peak position/ cm^{-1}**	**Assignment**
520	DMC	519	DMC
--	--	693	DMC
721	EC	717	EC
--	--	730	PF_6^- [2]
740	PF_6^- [2]	742	PF_6^- [2]
899	EC	894	EC
--	--	905	EC
--	--	916	DMC
--	--	934	
978	DMC or EC	974	DMC or EC
1082	EC	--	--
1119	DMC	--	--
1167	DMC	--	--
1221	EC	1223	EC
1374	EC	--	--
1467	DMC	1459	DMC
1485	EC	1486	EC
--	--	1753	DMC
1760	DMC	1776	DMC
1805	EC	1803	EC
2612	---	--	--
2732	EC	--	--
2850	DMC	2850	DMC
2890	DMC	2889	DMC
2938	EC	2935	EC
2966	DMC	2967	DMC
3002	EC	3006	EC
--	--	3038	DMC

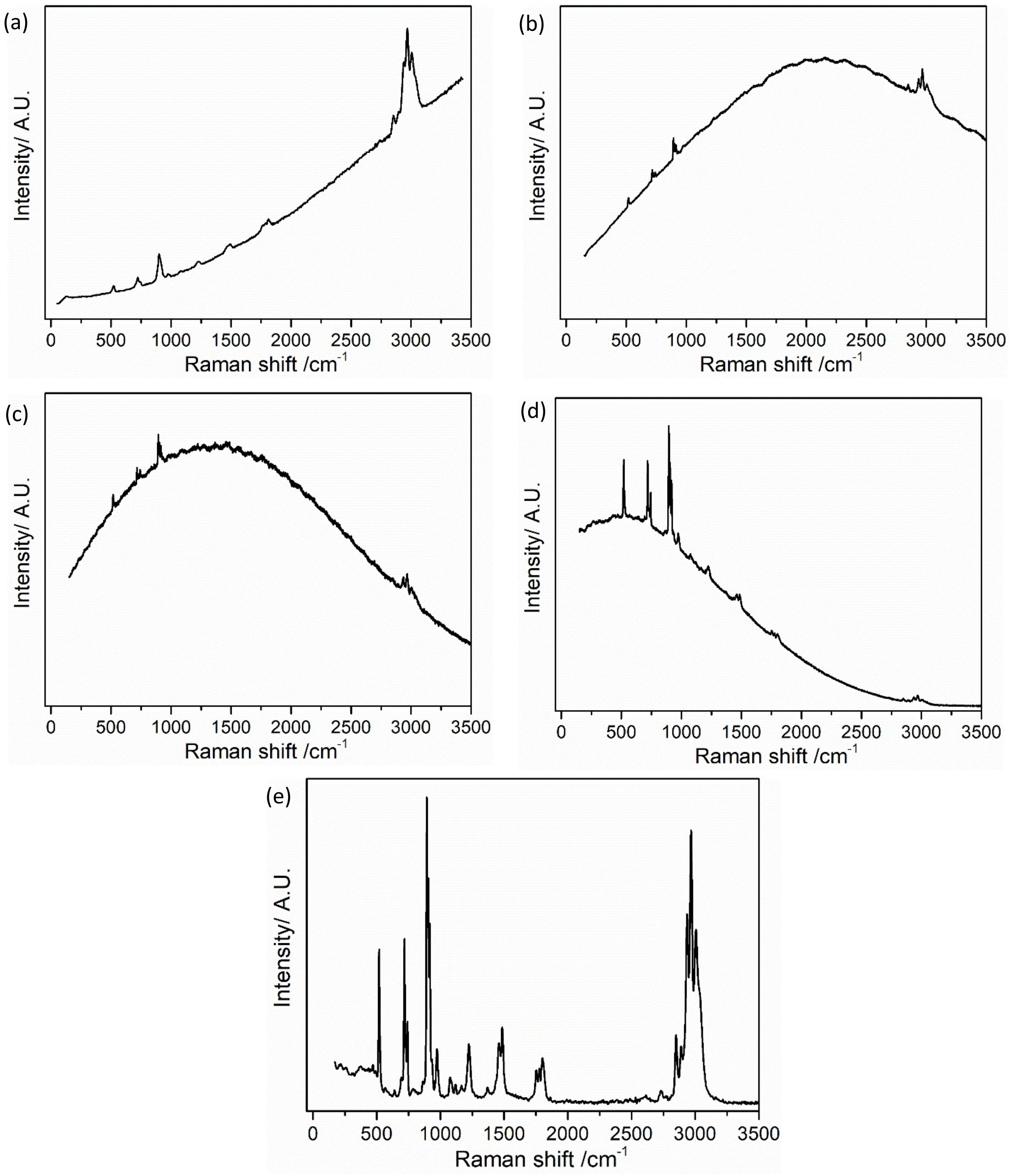

Figure S12 Comparison of (CW) Raman spectra of in-house prepared (non-commercial) electrolyte, 1 M $LiPF_6$ in EC/DMC 1:1 v/v, collected with laser (a) 400 nm, (b) 532 nm, (c) 633 nm, (d) 785 nm and (e) 1064 nm.

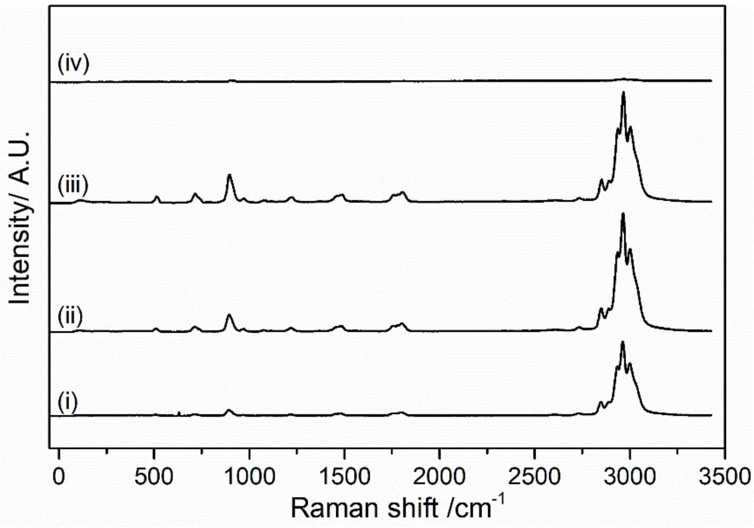

Figure S13. Kerr gate Raman spectra of of in-house prepared (non-commercial) electrolyte, 1 M $LiPF_6$ in EC/DMC 1:1 v/v. Spectra were collected at several delay times (i) -2 ps, (ii) 0 ps, (iii) 2 ps and (iv) 20 ps.

References

1 B. Valeur, *Molecular Fluorescence: Principles and Applications*, WILEY-VCH Verlag, 2001.

2 R. Aroca, M. Nazri, G. A. Nazri, A. J. Camargo and M. Trsic, Vibrational Spectra and Ion-Pair Properties of Lithium Hexafluorophosphate in Ethylene Carbonate Based Mixed-Solvent Systems for Lithium Batteries, *J. Solution Chem.*, 2000, **29**, 1047–1060.